5. FLUX VERSUS ANGLE-OF-INCIDENCE

Blistering-induced plasma impurity generation by high-energy fp bombardment is sensitive to the angle of incidence, as well as the particle flux. This effect has been modeled for prompt losses, including all the relevant particle drifts (neo-classical), motion along the magnetic field, and random gyro-phase.

5.1 Theory

The flux-per-steradian, $d\mathcal{F}/d\Omega$, at the wall is:

$$\frac{d\mathcal{F}}{d\Omega} = \frac{d\dot{n}}{dAd\Omega} = \int_V \frac{n_1 n_2 \langle\sigma v\rangle_{12} f_\ell(\Theta'_k \to \Theta'_{k+1}, \alpha_\ell \to \alpha_{\ell+1}) R dr d\Theta d\phi}{2\pi(\cos\alpha_\ell - \cos\alpha_{\ell+1})\Delta A} \tag{5.1}$$

Here $f_\ell(\theta'_k \to \theta'_{k+1}, \alpha_\ell \to \alpha_{\ell+1})$ is the differential loss fraction reaching the wall for $\theta'_k \leq \theta' \leq \theta'_{k+1}$, for angles of incidence $\alpha_\ell < \alpha < \alpha_{\ell+1}$, where

$$f_\ell(\theta'_k \to \theta'_{k+1}, \alpha_\ell \to \alpha_{\ell+1}) = f_\ell(\theta'_k \to \theta'_{k+1}) \times \rho(\Omega; \vec{r}_i)\Delta\Omega \ . \tag{5.2}$$

Details of the derivation are described in Appendix B. The function $\rho(\Omega; \vec{r}_i)$ is defined as the probability per unit angle that an alpha born at $\vec{r}_i$ will strike the wall with gyrophase angle Ω. It is found to be

$$\rho(\Omega;\vec{r}_i) = |1 - v_G \sin \Omega/v_D|/2\pi, \qquad (5.3)$$

where $\Omega = 0$ corresponds to grazing incidence when only gyromotion is considered. The velocities v_D and v_G are the radial components (in the wall frame) of the streaming-plus-drift motion and gyro-velocity, respectively. These velocities have been evaluated using expressions derived by Galeev and Sagdeev [14]. While the *integrand* of (5.1) is separable into a form like $f_\ell(\vec{r};\theta')\ \rho(\alpha,\theta';\vec{r})\ \langle\sigma v(\vec{r})\rangle$, the *integral* averages over all possible birth positions. Thus, the flux distribution is not separable into independent functions of α and θ', as done in Refs. 9 and 36. In particular, the spatial dependence of v_D/v_G must be included in this averaging process; this is discussed further below.

Recent analyses by Bauer et al. [9] and Belikov et al. [36] also consider this problem but use an average case probability distribution function (i.e. no spatial variation in v_D/v_G to calculate flux-versus-incidence-direction). For $v_D/v_G \ll 1$, $\rho(\Omega;\vec{r}_i)$ in Eq. (5.3) reduces to the linear probability function used in Ref. 9. While this assumption is good for reactor-sized machines, it breaks down for near-term devices that are of interest here. The present analysis includes spatial variations in v_D/v_G and yields fluxes as a superposition of sinusoidal profiles with significant fluxes at near-grazing incidence. This technique also allows for an offset, X_o, between the centers of

the plasma and wall cross sections (due to compression) and permits the poloidal wall radius to be arbitrarily larger than the plasma radius.

For particles to impact on the wall, the net radial velocity in the wall frame must be outward, yielding

$$\sin \Omega < v_D/v_G \equiv \sin \Omega_o. \tag{5.4}$$

The allowed range of gyrophase angles is then

$$0 \leq \Omega^* \leq \Omega < 2\pi + \Omega_o, \tag{5.5}$$

where Ω^* is defined by

$$(\Omega^*-\Omega_o)v_D/v_G = \cos\Omega_o - \cos\Omega^*. \tag{5.6}$$

When $v_G<v_D$, (5.3) remains valid, with $\Omega^* \leq \Omega \leq 2\pi$ and (5.6) being replaced by

$$\Omega^* v_D/v_G = 1 - \cos\Omega^*. \tag{5.7}$$

However, this case applies to a very small class of particles ($< 10^{-6}$ of total). Equations (5.6) - (5.7) are solved numerically using a Newton-Raphson search, with a starting guess for Ω^* of $(3\pi/2)-\Omega_o$.

Erosion due to sputtering by leaking background D-T ions can remove the surface so rapidly that build-up of a critical helium concentration and hence blistering, is prevented. (Sputtering by 3.5-MeV alphas is negligible [5] based on extrapolations of data by

Vernickel [37].) Bauer, et al. [9] first noted this problem, while Fenske et al. [38] have considered the θ'-dependence of alpha flux, found here for an average plasma edge temperature $\sim$ 60 eV. Reference 38 finds that blistering is possible for many materials for $20° \leq \theta' \leq 100°$, if the ratio of average alpha flux to background D-T flux is $\lesssim 0.1\%$. At other poloidal angles, D-T sputtering dominates (this is discussed further at the end of this chapter). In the present study, we have only considered blistering effects because in principle, improved plasma confinement and/or divertors can reduce D-T fluxes (and the consequent sputtering) to arbitrarily low levels. In this view, high-energy alpha losses represent a lower bound on wall-generated plasma impurities.

5.2 Results

Figures 5.1-5.4 show the results of our calculations for PLT, TFTR, ORNL-EPR and UWMAK-I. (See Table 5.1 for parameters). The resulting value of $dF/d\Omega$ rises from near zero at $\alpha = 90°$ (grazing), peaks at $\alpha = \alpha_c$ (some critical angle), then falls abruptly to zero for $\alpha < \alpha_c$. The rise in $dF/d\Omega$, as α decreases from 90° to α_c, is due to the sinusoidal probability distribution (c.f. eqn. (5.3)), since α varies sinusoidally in Ω, for $v_D/v_G \ll 1$. The abrupt drop in $dF/d\Omega$ occurs because $\alpha_c \simeq (\Omega^*)_{max}$ is determined by the maximum value of v_D/v_G from (5.6). In all cases, the peak value of $dF/d\Omega$ occurs at or near the poloidal wall position corresponding to the peak flux, F_{pk}.

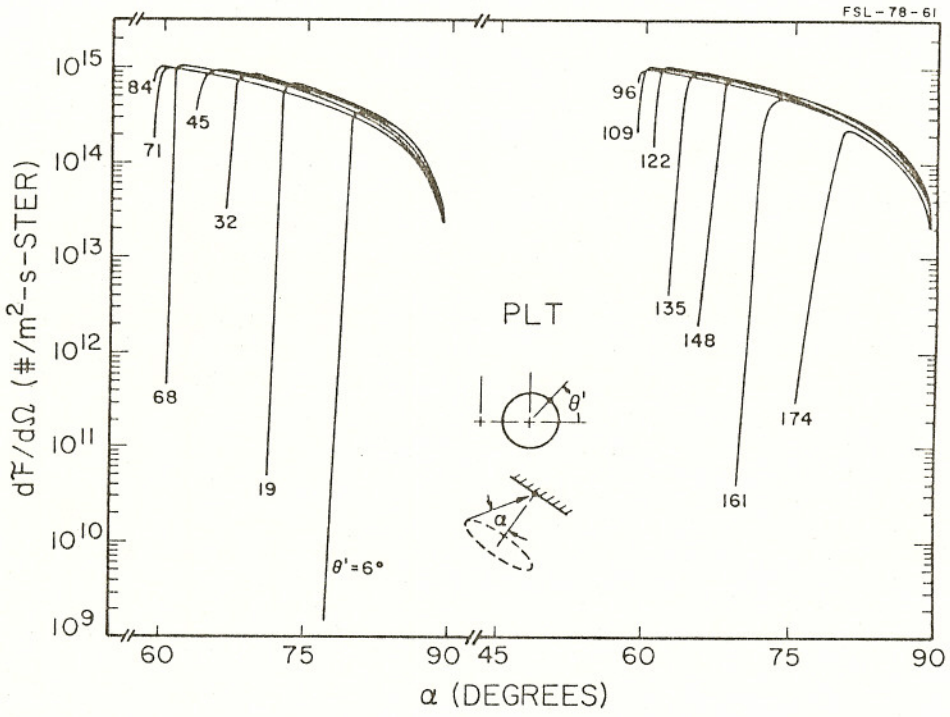

Figure 5.1 Flux of 3.5-MeV alphas versus incident velocity direction at various poloidal wall angles in PLT.

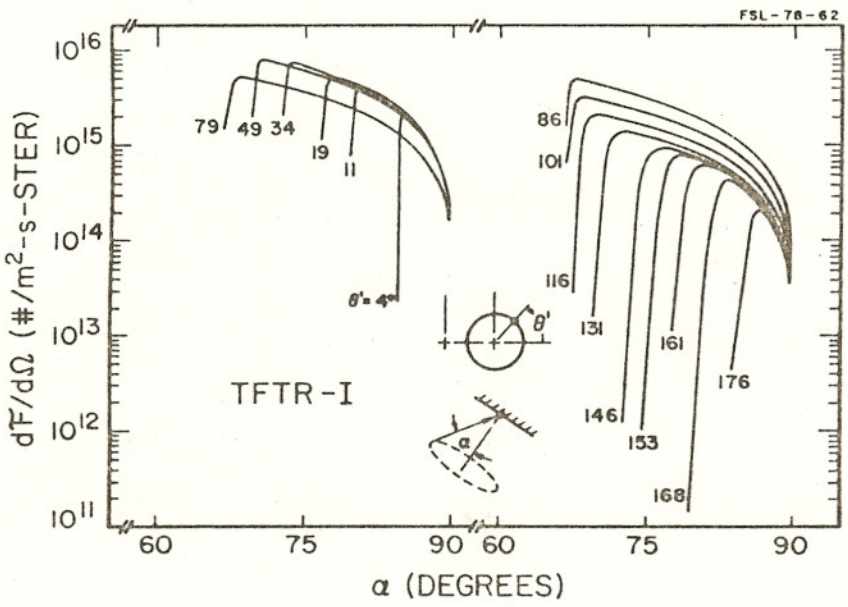

Figure 5.2 Flux of 3.5-MeV alphas versus incident velocity direction at various poloidal wall angles in TFTR-I.

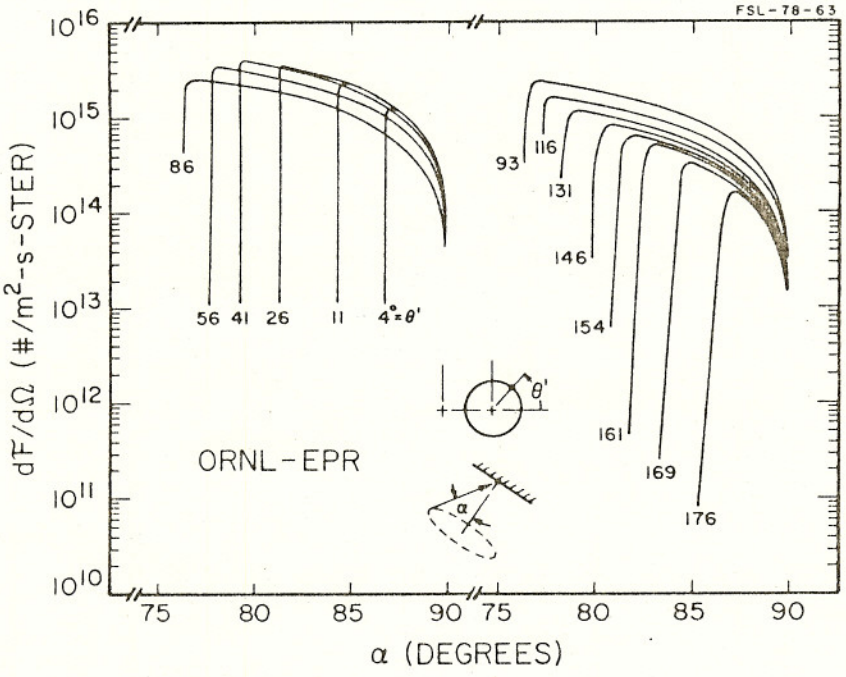

Figure 5.3 Flux of 3.5-MeV alphas versus incident velocity at various poloidal wall angles in ORNL-EPR.

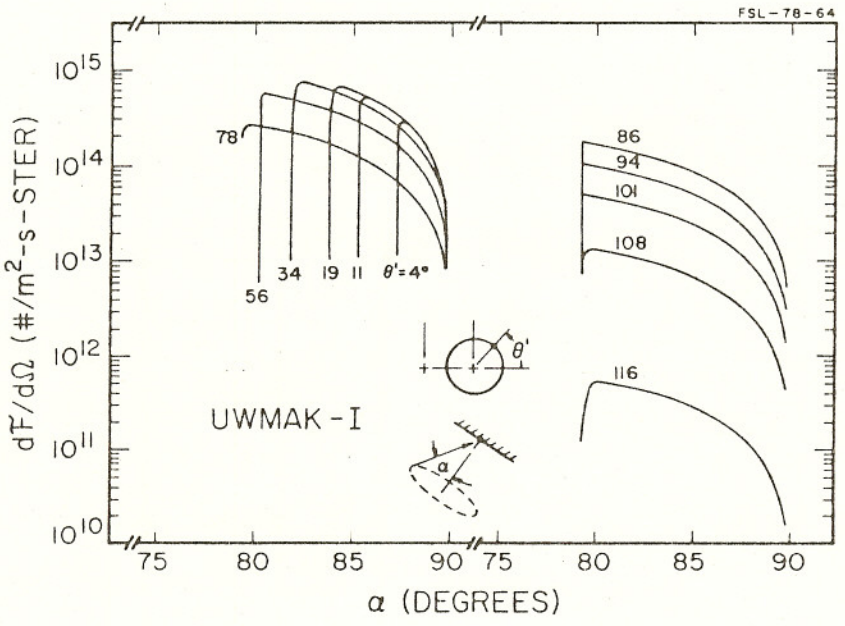

Figure 5.4 Flux of 3.5-MeV alphas versus incident velocity direction at various poloidal wall angles in UWMAK-I.

Table 5.1: Tokamak Parameters and Wall Loading Summary

Machine	PLT[26]	TFTR-I[27]$^{++}$	ORNL-EPR[28]	UWMAK-I[29]	JEPR[6]	T-20[7]
B_o(T)	4.6	5.2	4.8	3.82	4.0	3.5
I(MA)	1	1	7.2	21	3.67	6.09
R_o(m)	1.32	2.48	6.75	13.00	4.90	5.00
a(m)	0.45	0.54	2.25	5.00	1.50	2.00
r_w(m)	0.48	1.10**	2.25	5.50	1.50	2.00
T_{io}(keV)	5	10	22.5*	11.1	8	15
T_i/T_{io}	$1-.8(r/a)^2$	$1-.8(r/a)^2$	$1-(r/a)^2$	1	1	$1-(r/a)^2$
$n_{io}(m^{-3})$	$1x10^{20}$	$1.6x10^{20}$	$8x10^{19}$	$1.2x10^{20}$	$1.1x10^{20}$	$5x10^{19}$
n_i/n_{io}	$1-(r/a)^2$	$1-(r/a)^2$	$[1-(r/a)^2]^{\frac{1}{2}}$	$[1-.99(r/a)^2]^{\frac{1}{2}}$	$[1-(r/a)^3]^{\frac{1}{2}}$	$1-(r/a)^2$
J/J_o	$1-(r/a)^2$	$1-(r/a)^2$	$1-(r/a)^2$	1	1	$1-(r/a)^2$
F_ℓ	0.48	0.13	$3.1x10^{-3}$	$1.4x10^{-4}$	0.19	$3.3x10^{-3}$
F(#/m^2-s)	$1.1x10^{15}$	$4.5x10^{15}$	$1.5x10^{15}$	$1.6x10^{14}$	$3.1x10^{16}$	$2.1x10^{14}$
P/A$^+$	1.4	1.9	1.7	2.3	1.6	1.8

*An ignited system is assumed here, having a thermal power of 420 MW.

**There is also in offset of X_o = 0.17 m for this case.

+P/A is the ratio of peak-to-average alpha flux.

++This is the high compression senario in TFTR; the high current case is discussed in Ref. 4.

5.3 Application

To illustrate the significance of these results, blistering-induced plasma impurity generation has been estimated via a model developed by Fenske et al. [38]. A Thomas-Fermi form of nuclear-stopping, along with Brice's [39] electronic-stopping formula, are used to calculate the average projected range and straggling of 3.5-MeV alphas. The rate of helium concentration increase in near-surface regions of a steel first wall is obtained as a function of θ' and depth into the wall assuming a Gaussian projected range profile.

Under the assumption that prompt alpha losses dominate blistering formation (i.e., neglecting intermediate energy alphas, synergistic effects, etc.), the onset of rupture and flaking is taken to occur at a critical helium concentration value, taken here as 30 atomic-percent. The corresponding onset time is t_o, with a blister thickness equalling the depth of peak concentration, x_{pk}. The values of t_o and x_{pk} vary with poloidal wall angle; for example in ORNL-EPR, the maximum x_{pk} is 1 μm at $\theta' = 86°$ (see Fig. 5.5). The smallest onset time is $t_o \sim 4000$ hours at $\theta' = 56°$. Thus exfoliation begins at $\theta' = 56°$ in ORNL-EPR and gradually spreads to other θ'-values.

The average rate of impurity generation, $\dot{n}_I$, after many burn cycles (i.e., after sufficient operation so that blisters cover the whole surface area) is

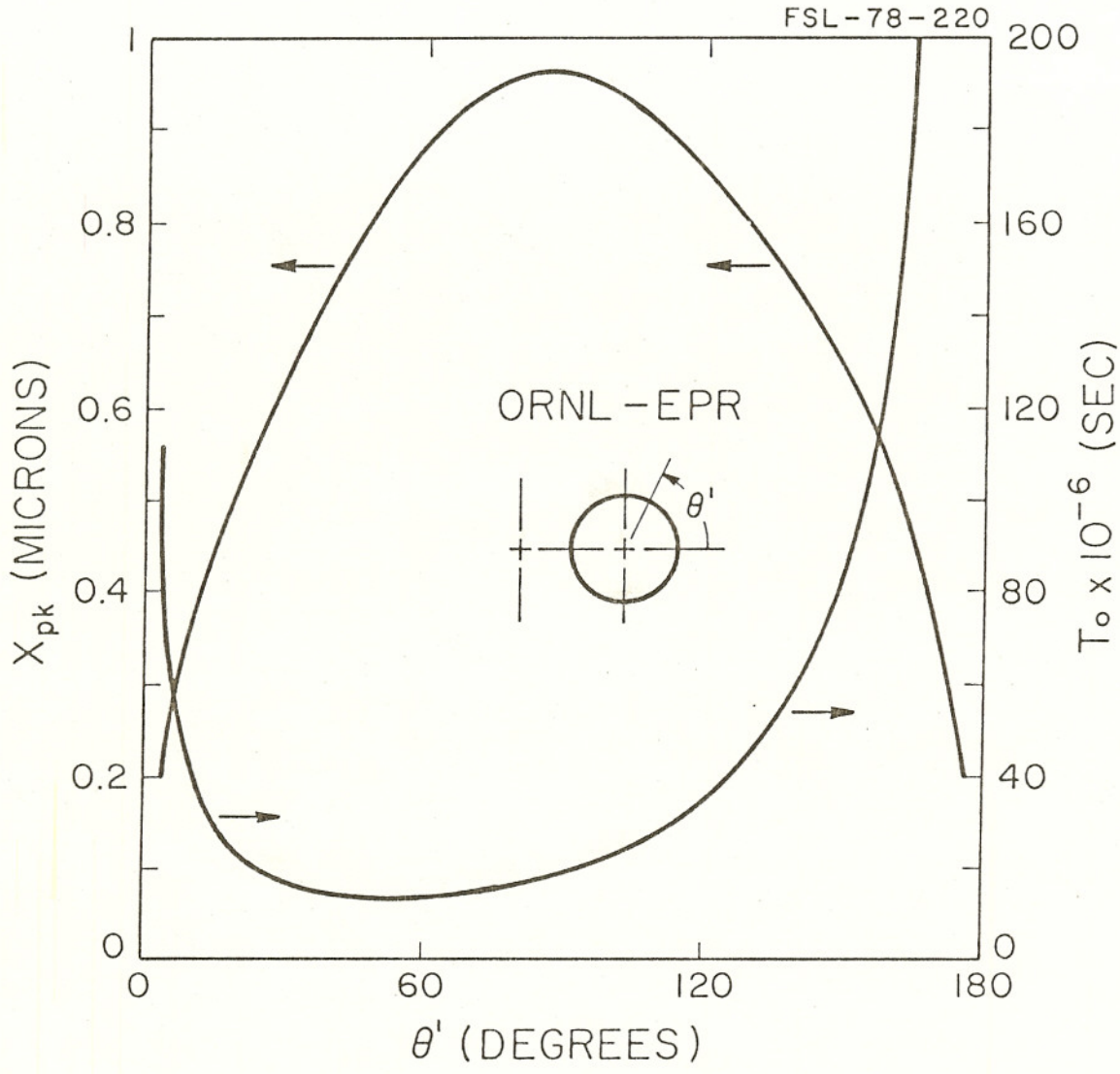

Figure 5.5 Depth, x_{pk}, of peak helium concentration and onset time, t_o, for blistering as a function of poloidal wall angle, θ', in ORNL-EPR (taken from Ref. 38).

$$\dot{n}_I = \frac{A_v f_s}{V f_t} \int \frac{x_{pk} dA}{t_o} \quad . \tag{5.8}$$

Here, $\int dA$ is taken over the upper (or lower) half of the wall area, and V is the plasma volume. Also, A_v is the atomic volume of iron; f_s is the fraction of the blistered surface which reaches the plasma as impurities (here taken as unity); f_t is the fraction of the onset time, during which flaking occurs (taken as 0.1, based on Fig. 11 of Ref. 40).

The effect of blistering-induced impurities must be evaluated by transport modeling. However, the most sophisticated models are inadequate to describe experimental results, even when neoclassical as well as anomalous terms are included [41]. Here, a global model is used:

$$\frac{\partial n_I}{\partial t} = \dot{n}_I + n_I/\tau_I, \tag{5.9}$$

where τ_I is the particle transport time. Depending on the details of the model (including boundary conditions), τ_I can be either positive or negative [41]. Consequently, the extreme case is assumed: all the impurities remain in the plasma ($\tau_I = \infty$), trivially yielding $n_I = \dot{n}_I t$. The accumulating impurities can then quench the burn by replacing D-T ions, assuming fixed β and fully stripped low-Z impurities. The characteristic time, τ_L, for

quenching the burn corresponds to the fusion rate decreasing to 1/e of its nominal value. The resulting time is:

$$\tau_L = 0.393\ \bar{n}_e/(Z_I+1)\dot{n}_I\ , \qquad (5.10)$$

where Z_I is the impurity charge, and $\bar{n}_e$ is the average electron density. Typical results of this calculation, shown in Table 5.2 for ORNL-EPR and UWMAK-1, indicate that $\tau_L < \tau_{burn}/2$ for a steel wall.

Table 5.2: The Effect of Blister-Injected Impurities

Parameter	ORNL-EPR	UWMAK-I
$\bar{n}_e(m^{-3})$	$4x10^{19}$	$8x10^{19}$
$\tau_{burn}(s)$	100	5400
$\tau_L(s)$	47	2310
$\Delta_W(\tau_L = 10\tau_b)$	0.17	0.028
$\Delta_W(\tau_L = 20\tau_b)$	0.20	0.031
$\Delta_I(\tau_L = 10\tau_b)$	0.92	0.26
$\Delta_I(\tau_L = 20\tau_b)$	1.23	0.29

Fenske et al [38] have examined the combined effect of MeV α-blistering (using the spatial and angle-of-incidence profiles obtained in the present work) and thermal D-T sputtering on impurity generation. Figure 5.6 shows the resulting impurity level in ORNL-EPR [normalized to the impurity level due to a D-T flux of $5x10^{17}$ ions/(m^2-s)] versus accumulated reactor operating time.

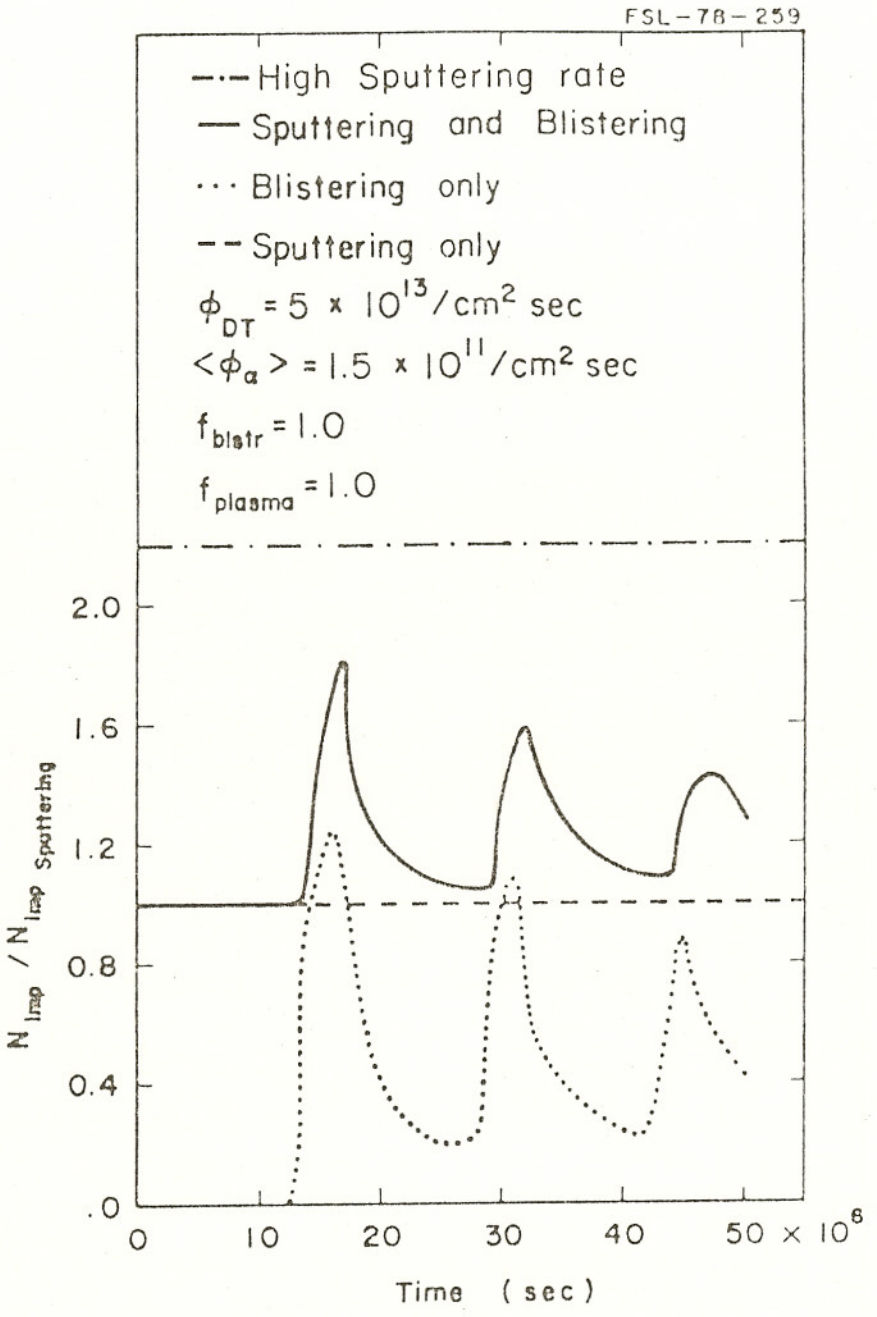

Figure 5.6 Impurity levels in ORNL-EPR are plotted versus accumulated operating time (taken from Ref. 38).

The dotted curve in Fig. 5.6 assumes only blistering-injected impurities, while the dashed line indicates the sputtering-induced impurity level. The solid line shows the impurity level due to blistering and simultaneous D-T sputtering, accounting for increased blister formation time, as well as the decreased blister-skin thickness. Increasing the D-T flux reduces the relative effect of blistering until the surface is eroded by sputtering at a rate too fast to allow blister formation. This trend is shown by the chain-dotted curve in Fig. 5.6. These results show that the combined effect of blistering and sputtering typically produces $\lesssim$ 50% increase in the impurity generation rate over blistering alone, potentially limiting the burn time to $\tau_L < \tau_{burn}/3$. Thus, it is concluded that blistering by MeV alphas, with or without DT sputtering, might reduce the burn time by 50-70%.

The surface heating effect of MeV alphas and keV DT ions is not included in this analysis. A comprehensive review of plasma-wall interactions, including such effects, has been done recently by McCracken and Stott [122].